In situ neutron diffraction study of the high-temperature redox chemistry of Ln3–xSr1+xCrNiO8–δ (Ln = La, Nd) under hydrogen

Florent Tonus, Mona Bahout, Peter D. Battle, Thomas Hansen, Paul F. Henry, Thierry Roisnel

In situ neutron diffraction study of the high-temperature redox chemistry of $Ln_{3-x}Sr_{1+x}CrNiO_{8-\delta}$ (Ln = La, Nd) under hydrogen†

Florent Tonus,[a] Mona Bahout,*[a] Peter D. Battle,*[b] Thomas Hansen,[c] Paul F. Henry[d] and Thierry Roisnel[a]

Received 14th December 2009, Accepted 17th March 2010
First published as an Advance Article on the web 9th April 2010
DOI: 10.1039/b926282b

The chemical reduction of the K_2NiF_4-type oxides, $Ln_2Sr_2CrNiO_{8-\delta}$ (Ln = La, Nd) and $Nd_{2.25}Sr_{1.75}CrNiO_{8-\delta}$, has been investigated *in situ* under a dynamic hydrogen atmosphere at high temperature using neutron powder diffraction. The high count-rate and high resolution of the D20 diffractometer at ILL, Grenoble allowed real-time data collection and structure refinement by full-pattern Rietveld analysis with a temperature resolution of 1 °C. Excellent agreement was obtained with the results of thermogravimetric analysis of these materials, which are potential fuel-cell electrodes. The neutron study revealed that oxygen is lost only from the equatorial anion site; the reduction of $La_2Sr_2CrNiO_{8-\delta}$ yields a pure Ni(II) phase, $La_2Sr_2CrNiO_{7.5}$ *en route* to a mixed Ni(II,I) oxide, $La_2Sr_2CrNiO_{7.40}$, whereas hydrogen reduction of $Nd_2Sr_2CrNiO_{8-\delta}$ and $Nd_{2.25}Sr_{1.75}CrNiO_{8-\delta}$ proceeds continuously from Ni(III) to an average oxidation state of 1.80 for the nickel ion. The data collected throughout a subsequent heating/cooling cycle in air indicated that the reduced phases intercalate oxygen reversibly into the equatorial vacancies of the K_2NiF_4-type structure. The retention of $I4/mmm$ symmetry, along with the absence of the formation of any impurities throughout the heating/cooling cycles under reducing and oxidizing atmospheres, demonstrates both the reversibility and the strongly topotactic character of the oxygen deintercalation/intercalation chemical redox process and establishes the excellent structural stability of these layered mixed-metal oxides over a wide range of oxygen partial pressures.

Introduction

Energy-related materials in electrochemical devices such as solid oxide fuel cells (SOFCs) are inevitably placed in chemically severe environments. They should exhibit good stability under steep temperature gradients and a wide range of oxygen partial pressure. The most common anode materials in SOFCs are Ni–YSZ cermets, which consist of metallic nickel particles and an yttria-stabilized zirconia skeleton. These display excellent catalytic properties for fuel oxidation and good current collection, but they do have serious disadvantages, for example poor redox tolerance and long-term instability, which preclude many medium- and large-scale applications. Extensive studies to find alternative anode materials with various structure types have been undertaken.[1,2] For example, the doping of $LaCrO_3$-based perovskites with various 3d elements has been investigated in an attempt to improve the conductivity and electrocatalytic properties of the parent compound.[3–5] Of the various dopants, nickel seemed to be the most successful, although significant Ni-metal leaching occurred under working conditions even when the Ni-doping at the B-site was as low as 10%.[6] The possibility that the activity of these materials is due to surface leaching of nickel metal raises questions about their long-term stability as anode materials.

The need for materials that are more stable under reducing conditions has recently stimulated the study of mixed-metal oxides belonging to the Ruddlesden–Popper (RP) series of compositions, $A_{n+1}B_nO_{3n+1}$. The K_2NiF_4-like structure adopted by the $n = 1$ RP oxides consists of perovskite-like sheets of composition BO_2, separated from each other by two rock-salt-like layers of composition AO, giving a formula A_2BO_4. The oxide ions within the perovskite and rock-salt layers are said to occupy respectively equatorial and axial sites around the cation B. The structure can accommodate either excess oxygen ($+\delta$) in interstitial sites within the rock-salt layers or oxygen vacancies ($-\delta$) within the perovskite layers, hence leading to the formulation $A_2BO_{4\pm\delta}$. As a consequence of their structural flexibility, some K_2NiF_4-type oxides have shown an enhanced thermal stability under a reducing atmosphere of hydrogen gas.[7,8] We have recently introduced a combination of nickel and chromium into the K_2NiF_4 structure by synthesizing $Ln_{3-x}Sr_{1+x}CrNiO_{8-\delta}$ (Ln = lanthanide; $0.1 \leq x \leq 1$)[9] with the aim of identifying potential anode materials for SOFCs. Our approach of selecting Cr/Ni-based compositions was influenced by the relative success of the analogous perovskite system described above. This stems firstly from the stability of Cr^{3+} to hydrogen reduction and the structural stability that this confers. Secondly, it relies on the

[a]*Université de Rennes 1, Laboratoire Sciences Chimiques de Rennes, UMR CNRS 6226, 263 avenue du général Leclerc, 35402 Rennes CEDEX, France. E-mail: mona.bahout@univ-rennes1.fr*
[b]*Inorganic Chemistry Laboratory, Department of Chemistry, University of Oxford, South Parks Road, Oxford, OX1 3QR, UK. E-mail: peter.battle@chem.ox.ac.uk*
[c]*Institut Laue Langevin, 6 rue Jules Horowitz, BP156, 38042 Grenoble CEDEX 9, France*
[d]*MI-1, Helmholtz Zentrum Berlin, Hahn-Meitner-Platz 1, 14109 Berlin, Germany*

† Electronic supplementary information (ESI) available: Additional TGA and structural data. See DOI: 10.1039/b926282b

electrocatalytic properties of the Ni cation and its ability to lower its oxidation state and coordination number in order to generate the oxygen-vacancy network needed for anionic conduction. Thermogravimetric analysis (TGA) in 5% H_2 on various $Ln_{3-x}Sr_{1+x}CrNiO_{8-\delta}$ compositions has demonstrated that hydrogen reduction yields oxygen-deficient phases which exhibit excellent stability under a dry H_2 atmosphere up to 900 °C.[10] In order to ensure mechanical compatibility at the electrode/electrolyte interface in SOFCs, knowledge of the thermal expansion and structural behaviour of the component materials under the appropriate atmosphere at high temperature is essential. In this paper we describe a study of the high-temperature structural chemistry of some potential anode materials under reducing conditions.

Taking advantage of the sensitivity of neutron diffraction to light atoms, we have previously modified the sample environment on the D20 powder diffractometer at ILL, in order to monitor *in situ*, and in real time, the structural behavior of $Pr_2Sr_2CrNiO_{8-\delta}$ in a dynamic hydrogen atmosphere at high temperature.[11] We showed that $Pr_2Sr_2CrNiO_{8-\delta}$ (*i.e.* $PrSrCr_{0.5}Ni_{0.5}O_{4-\delta}$) retained the K_2NiF_4 structure under strong reducing conditions (5% H_2 at 700 °C); the Ni^{3+} cations were reduced to Ni^{2+} forming $Pr_2Sr_2CrNiO_{7.50}$. Our neutron powder diffraction (NPD) experiments clearly established that the reduction reaction involved removal of oxygen only from the equatorial positions and that no redistribution of the remaining oxygen atoms occurred between the different sites (equatorial, axial, interstitial) during the reduction or when the reduced sample was held at 400 °C before cooling to room temperature. Subsequent heating in oxygen reoxidised the sample, again with retention of the K_2NiF_4 structure.

In an attempt to investigate the influence of the lanthanide cation and the Sr-doping level, we have now performed similar experiments under flowing 5% H_2 on three further compositions, $Ln_2Sr_2CrNiO_{8-\delta}$ (Ln = La, Nd) and $Nd_{2.25}Sr_{1.75}CrNiO_{8-\delta}$, up to 700 °C. The results of these experiments are described below. Similar *in situ* investigations performed on mixed (Mn, Cr) compositions will be reported elsewhere.

Experimental

(i) Synthesis

Polycrystalline $Ln_{3-x}Sr_{1+x}CrNiO_{8-\delta}$ (Ln = La, Nd) samples were prepared by a solution route which efficiently produces powder with high chemical homogeneity. La_2O_3 and Nd_2O_3 (99.99% Alfa Aesar) were overnight heated in air at 900 °C to remove adsorbed water, hydroxide or carbon dioxide. The lanthanide oxide was dissolved in a concentrated nitric acid solution (pH = 2). Stoichiometric quantities of Sr-, Cr- and Ni-acetates (99.99% Aldrich) were then added to the solution which was heated at ~130 °C with constant stirring until a gel formed. Subsequent heating to ~250 °C removed water and caused the gel to form a dry resin. Heating the resin at ~550 °C overnight decomposed the organic precursors. The resulting powder was ground and pressed into pellets (2 mm thickness, 13 mm diameter) which were annealed in an alumina crucible for ~48 h at ~1250 °C under flowing argon which had been dried by passage over concentrated sulfuric acid. The sample was then cooled to room temperature at a rate of 2 °C min^{-1} under the argon flow. In order to avoid any loss of reactants due to their reactivity with alumina, direct contact with the crucible was prevented by surrounding the pellets by a powder 'blanket' of the same composition. The optimum synthesis conditions for the reduced compositions were established from thermogravimetric studies.

(ii) Thermal behavior

Thermogravimetric analysis (TGA) was carried out using a Setaram TGDTA 92. Samples, weighing ~100 mg, contained in quartz crucibles, were placed in the apparatus which was purged for 30 min with 5% H_2/N_2. Samples were subsequently heated up to 800 °C under the gas flow before being allowed to cool to room temperature, also under the gas flow. The reduced samples were then heated to 500 °C under flowing oxygen and held at that temperature for 3 h before being cooled to room temperature, still under the gas flow.

(iii) Determination of the oxygen content

The oxygen deficiency δ in $Ln_{3-x}Sr_{1+x}CrNi^{2+}{}_{1-\tau}Ni^{3+}{}_{\tau}O_{8-\delta}$ is correlated to the Ni^{3+}-content τ, with $\delta = (x - \tau)/2$. The Ni^{3+}-content was determined by iodometric titration against a sodium thiosulfate solution[12] which had been standardized against potassium iodate.[13] The values reported in Table 1 have been determined from ~50 mg polycrystalline samples dissolved in 20 mL of 12 M hydrochloric acid in a closed, argon-filled apparatus. Care was taken to achieve complete dissolution of the sample and to prevent any chlorine escape or oxygen entry as the latter quickly oxidizes iodide, resulting in an overestimation of the oxygen content. The value of δ was determined with an accuracy of ±0.02. The analytical method was validated using an $Nd_2NiO_{4+\delta}$ sample with known oxygen content ($\delta = 0.24$).

(iv) X-Ray powder diffraction (XRD)

X-Ray powder diffraction patterns were recorded with a Bruker D8 Discover diffractometer (Cu $K\alpha_1$ radiation, $10 \leq 2\theta^\circ \leq 130$, step size = 0.008°, 1.4 s per step, Lynx Eye detector). Rietveld refinement was carried out using FullProf program suite.[14] Two asymmetry parameters were refined below $2\theta = 35°$ and 30-point

Table 1 Lattice parameters and oxygen content of $Ln_{3-x}Sr_{1+x}CrNiO_{8-\delta}$ before and after reduction

	As-prepared	After reduction	Reoxidized in air
$La_2Sr_2CrNiO_{8-\delta}$			
δ^a	0.13(2)	0.50(5)	0.02(2)
a/Å	3.829655(6)	3.842291(6)	3.82853(5)
c/Å	12.63454(2)	12.602626(2)	12.6327(4)
$Nd_2Sr_2CrNiO_{8-\delta}$			
δ^a	0.15(2)	0.60(5)	0.01(2)
a/Å	3.800267(8)	3.79801(1)	3.798845(5)
c/Å	12.47105(3)	12.46457(3)	12.47517(2)
$Nd_{2.25}Sr_{1.75}CrNiO_{8-\delta}$			
δ^a	0.13(2)	0.45(5)	−0.09(2)
a/Å	3.80808(4)	3.81679(6)	3.802009(6)
c/Å	12.4314(1)	12.4119(2)	12.46527(3)

[a] δ determined iodometrically for the as-prepared and reoxidized samples, the additional oxygen loss on reduction determined by TGA.

interpolated backgrounds were used. A pseudo-Voigt peak shape function was used together with an anisotropic peak broadening function which allows the width of a Bragg reflection to depend on the Miller indices *hkl*.[15,16]

(v) *In situ* neutron powder diffraction

In situ neutron diffraction experiments were carried out on three samples, $Ln_2Sr_2CrNiO_{8-\delta}$ (*Ln* = La, Nd) and $Nd_{2.25}Sr_{1.75}CrNiO_{8-\delta}$, on the high-flux, two-axis neutron powder diffractometer D20[17] at the Institut Laue Langevin (ILL) Grenoble, France according to the strategy described previously.[11] A take-off angle of 118° from the (115) plane of a germanium monochromator was chosen, giving a wavelength of $\lambda = 1.8682$ Å and a resolution of $\Delta d/d \approx 3 \times 10^{-3}$, while retaining a high flux on the sample ($\sim 10^7$ n cm^{-2} s^{-1}). Slits were used to define the beam to be 30 mm high and 15 mm wide at the sample position. High-temperature measurements under flowing H_2 gas required the modification of the standard sample environment. In the case of the neodymium-containing compounds, the powder sample (~0.5 g) was loaded in a 10 mm diameter quartz tube between two pieces of quartz wool which allowed unrestricted gas flow through the sample, while also being the support. In the case of $La_2Sr_2CrNiO_{8-\delta}$ the sample was contained in a glass tube of 8 mm diameter, closed at the bottom and open at the top, in an attempt to achieve a configuration similar to that of the TGA equipment. The tube was mounted in the standard D20 furnace and connected to a flow of reducing gas (5% H_2/He) which was controlled by a needle valve connected to a Bourdon gauge. The sample position was marked so as to follow any movement during the experiment under the positive pressure of gas; no sample movement was detected once the overpressure range had been determined. The overpressure was set at approximately 20–25 mbar at room temperature and monitored over the full temperature range to ensure a regular gas flow. The quartz tube was centered in the beam with centering rings top and bottom, and also by a boron nitride collar housing the control thermocouples which was situated just below the beam window. The furnace element was a 22 mm diameter vanadium-foil cylinder with two further outer vanadium-foil shields (26 and 30 mm diameter) to reduce power consumption and provide a homogeneous temperature environment. The furnace temperature was raised to ~700 °C with a heating rate adjusted to be between 1 and 5 °C min^{-1} over the temperature range where significant weight loss was anticipated on the basis of TGA data. The sample was then cooled, under flowing gas, to room temperature at 25 °C min^{-1}. The temperature was calibrated off-beam with a type-K thermocouple located in the centre of the furnace, which otherwise retained the same configuration as during the last data collection. Diffraction patterns were collected throughout the heating and cooling cycle; a pattern took ~1 min to collect, giving a maximum temperature resolution of 1 °C. The number of diffraction patterns collected below the transition temperature was lower for the Nd-containing samples than for $La_2Sr_2CrNiO_{8-\delta}$ because a faster heating rate was used (5° *vs.* 1 °C min^{-1}). In addition to these time-resolved data, diffraction patterns were collected at appropriate temperatures selected on the basis of previous TGA experiments, *i.e.* just before and after the reduction process (at $T \approx 250$ °C and $T \approx 450$ °C, respectively) as well as at the upper temperature attained in the neutron experiment, $T \approx 700$ °C. For two samples, in order to check the stability in air and assess the reversibility of the oxygen loss, the reduced phase was subsequently heated in air at 5 °C min^{-1} to ~500 °C and then cooled to room temperature at 25 °C min^{-1} with a full diffraction pattern being collected every minute. Structural analysis was performed by the Rietveld method[14,18] using the FullProf program.[19] In order to ensure a good background correction, a diffraction pattern was collected for 1 h at room temperature from the quartz tube and the glass wool support. This background contribution was then normalised to the incident monitor count so that it could be subtracted from the shorter-timescale raw data without introducing significant noise. The remaining background as a consequence of the quartz tube contribution was subsequently treated using a Fourier filtering technique and the peak shapes were modeled using a pseudo-Voigt function with two peak asymmetry parameters refined below $2\theta = 30°$.

Results and discussion

(i) Synthesis

The temperature and gas atmosphere were found to be crucial in obtaining pure K_2NiF_4-type compounds. The difficulty in forming single-phase materials in air is due to the competitive formation of Ln_2O_3 and chromate impurity phases (*e.g.*, $SrCrO_4$). Successful synthesis of $Ln_{3-x}Sr_{1+x}CrNiO_{8-\delta}$ compositions must be carried out in an oxygen-free atmosphere, in the temperature range 1200–1350 °C. X-Ray diffraction showed that the $Nd_2Sr_2CrNiO_{8-\delta}$ and $Nd_{2.25}Sr_{1.75}CrNiO_{8-\delta}$ samples were single-phase materials whereas the $La_2Sr_2CrNiO_{8-\delta}$ sample contained a small quantity of a $SrCO_3$ impurity. The level of impurity present in the $La_2Sr_2CrNiO_{8-\delta}$ sample studied by *in situ* NPD was estimated to be 0.74 wt% by TGA. It was poorly crystalline and the concentration could consequently not be quantified from XRD.

(ii) Oxygen content and thermogravimetric analysis (TGA)

The oxygen content of our as-prepared $Ln_{3-x}Sr_{1+x}CrNiO_{8-\delta}$ samples, as determined by iodometric titration of Ni^{3+}, is lower than the ideal stoichiometric value; $0.13 \leq \delta \leq 0.15$. Similar analyses performed on samples of $La_2Sr_2CrNiO_{8-\delta}$ and $Nd_2Sr_2CrNiO_{8-\delta}$ that had been reduced in flowing 5% H_2 at 700 °C for 8 h and then reoxidized in air at ~500 °C for 5 h showed no significant oxygen deficiency (Table 1). When a sample of $Nd_{2.25}Sr_{1.75}CrNiO_{8-\delta}$ was treated in the same way, the reoxidised sample showed an oxygen excess, implying that some interstitial sites are occupied and that the mean oxidation state of nickel is consequently increased to 2.93. The nickel oxidation state in all our compounds thus approaches Ni^{3+} in an oxygen-rich environment. The oxygen deficiency in our as-prepared $Ln_{3-x}Sr_{1+x}CrNiO_{8-\delta}$ samples is consistent with previous results on highly Sr-doped, $(Ln,Sr)_2NiO_4$-type oxides,[20] and is a consequence of the difficulty of stabilizing the Ni^{3+} oxidation state at high temperature under an argon atmosphere; very high oxygen pressures (150–600 kbar) are often required to stabilize the Ni^{3+} oxidation state at high temperatures in perovskites[21,22] and K_2NiF_4-type oxides.[23,24] The oxygen deficiency

contrasts with the oxygen excess found in the compositions $Ln_2NiO_{4+\delta}$ in which nickel is the only transition metal and the *A* site is occupied only by a lanthanide cation. The excess oxygen in these compositions provides structural stability whilst inducing the oxidation of Ni^{2+} to Ni^{3+}.[25,26] The level of interstitial oxygen is reduced by Sr-doping[27,28] because the greater size of Sr^{2+} with respect to La^{3+} gives additional stability.

It proved impossible to confirm the oxygen contents established from iodometry by means of thermogravimetric analysis under 5% H_2, because complete decomposition of the samples to Ln_2O_3, Cr_2O_3, SrO and Ni-metal did not occur under the conditions used. The weight-loss curve of $La_2Sr_2CrNiO_{8-\delta}$ exhibits two well separated steps, at ~400 and ~650 °C. The TG curves of $Nd_2Sr_2CrNiO_{8-\delta}$ and $Nd_{2.25}Sr_{1.75}CrNiO_{8-\delta}$ show a single step at ~400 °C (Fig. 1 and S1†) with inflection points sometimes visible at ~600–650 °C, depending on the sample batch and heating rates used. The first weight loss observed for $La_2Sr_2CrNiO_{8-\delta}$ (~0.88 wt%) corresponds to loss of 0.38 oxygen per f.u., resulting in the Ni(II)-composition, $La_2Sr_2CrNiO_{7.50(5)}$. It is difficult to determine accurately the oxygen loss within the second mass loss as it also involves some contribution from the $SrCO_3$ impurity which should decompose to SrO in this temperature range.[29] However, the quantity of $SrCO_3$ is insufficient to account for all of the second weight loss. Hydrogen reduction of the $Nd_2Sr_2CrNiO_{8-\delta}$ and $Nd_{2.25}Sr_{1.75}CrNiO_{8-\delta}$ samples consists of loss of 0.44 and 0.30 oxygen per f.u. resulting in mixed valence Ni(II,I)-compositions $Nd_2Sr_2CrNiO_{7.40(5)}$ and $Nd_{2.25}Sr_{1.75}CrNiO_{7.55(5)}$, respectively, which are stable up to ~800 °C.

The thermal stability of the layered (Cr,Ni) reduced oxides, $Ln_{3-x}Sr_{1+x}CrNiO_{8-\delta}$, is thus intermediate between the behavior of the pure Ni and Cr-phases; the former are completely decomposed in dilute H_2 below ~700 °C[30,31] while the latter do not lose any oxygen up to 1000 °C, even under pure H_2.[32]

The reduced $Ln_{3-x}Sr_{1+x}CrNiO_{8-\delta}$ oxides are not air sensitive at room temperature, as was confirmed by the absence of any change in the XRD patterns of samples exposed to the air for up to several months. This behavior contrasts to the high reactivity of the anion-deficient perovskites $LaSrCr_{0.6}Ni_{1.4}O_{3-\delta}$ that reoxidise within 2 hours under normal storage conditions.[33] However, the reduced $Ln_{3-x}Sr_{1+x}CrNiO_{8-\delta}$ samples start to take up oxygen rapidly at ~400 °C in air, although full oxidation is not complete after 3 h at ~500 °C (Fig. 1).

(iii) *Ex situ* XRD at RT before and after reduction

Preliminary structural studies were based on XRD data, which were collected over a period of several hours. Conventional Rietveld refinement was unable to fit properly the whole diffraction profile whatever the space group (*I*4/*mmm*, *Fmmm* or *Immm*) as strong anisotropic broadening of some Bragg reflections was observed. The peak width appeared to depend on the Miller indices of the reflection as well as on the scattering angle. In particular, Bragg peaks with strong *l* character were fitted relatively poorly compared to the other peaks. Rietveld analyses in the space group *I*4/*mmm*, with due allowance made for the presence of anisotropic microstrains, gave a satisfactory fit to the observed diffraction patterns. The unit cell parameters are listed

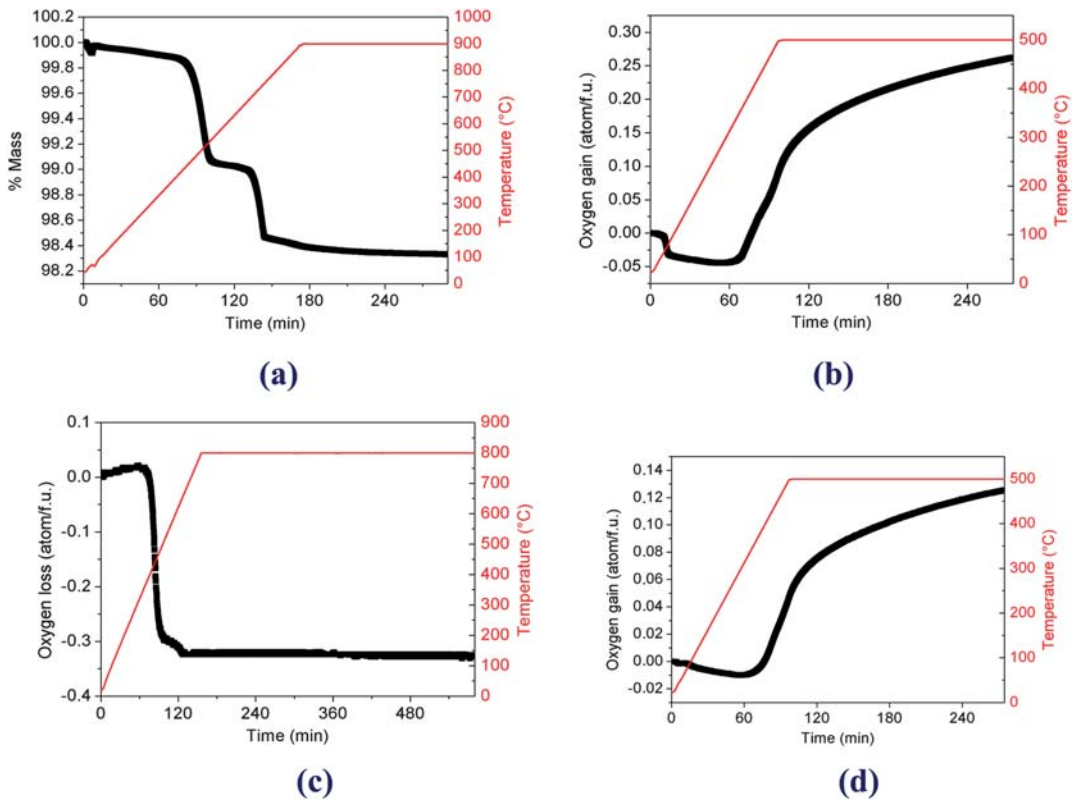

Fig. 1 Thermogravimetric data (heating rate of 5 °C min^{-1}) for (a) the reduction of as-prepared $La_2Sr_2CrNiO_{8-\delta}$ under 5% H_2 in N_2 and (b) reoxidation of the reduced material in O_2; (c) the reduction of as-prepared $Nd_2Sr_2CrNiO_{8-\delta}$ under 5% H_2 in N_2 and (d) reoxidation of the reduced material in O_2.

in Table 1; the values for $La_2Sr_2CrNiO_{8-\delta}$ are in good agreement with those reported previously by Millburn and Rosseinsky.[34] The standard deviations given in Table 1 and throughout this paper give an estimate of the precision of the parameter that is the minimum width of the confidence interval. Any unidentified systematic errors would cause the accuracy of the parameter to be somewhat lower.

X-Ray diffraction patterns taken from large-scale (~1 g) samples of $Ln_2Sr_2CrNiO_{8-\delta}$ (Ln = La, Nd) that had been reduced in 5% H_2/N_2 at 700 °C for 8 hours did not reveal the presence of any impurity phases. Structural refinements indicated that the reduced phases retain the *I*4/*mmm* space group (Fig. S2–S4†). The unit cell parameters of the reduced samples are included in Table 1. The X-ray diffraction patterns collected from samples that had been reduced and then reoxidized in air at ~550 °C for 5 hours also indicated retention of the *I*4/*mmm* space group and the absence of impurities. Rietveld refinements showed contraction of the lattice parameter *a* and an expansion of *c* (Table 1), in direct contrast to the behavior observed during the initial heating under hydrogen. This behavior suggests that the samples undergo reversible oxygen deintercalation/intercalation that is governed by the partial pressure of oxygen.

(iv) Neutron diffraction

NPD also indicated that, with the exception of the carbonate impurity in $La_2Sr_2CrNiO_{8-\delta}$, the as-prepared materials were single-phase with no evidence of symmetry lowering due to cation order which would have been difficult to detect in the XRD patterns. The scattering-length contrast between Cr and Ni is such that ordering would have been easily detected from the neutron data.[35] The structure was refined in space group *I*4/*mmm* in which Cr and Ni randomly occupy the six-coordinate 2*a* site (0, 0, 0) in a 1 : 1 ratio, in agreement with the expected composition. The atomic parameters varied in the structural refinements included the *z* coordinate of the (*Ln*/Sr) site and axial oxygen atom (O1), the anisotropic displacement parameters of all the atoms, and the occupancy factors of the axial and equatorial (O2) oxygen atoms. Refinement of the NPD diagrams collected at room temperature before reduction indicated a slight oxygen deficiency at the O2 (equatorial) position; the compositions refined to be $La_2Sr_2CrNiO_{7.87(2)}$, $Nd_2Sr_2CrNiO_{7.84(3)}$ and $Nd_{2.25}Sr_{1.75}CrNiO_{7.85(2)}$, in excellent agreement with iodometric analysis (Table 1). In the analysis of the diffraction pattern collected from the lanthanum-containing sample, due allowance was made for the presence of the $SrCO_3$ impurity. The structural behaviour of these three systems was monitored by NPD as the materials were heated (Ln = La, 1 °C min^{-1}; Nd, 5 °C min^{-1}) in flowing 5% H_2 up to ~700 °C then cooled to room temperature under the gas. No additional peaks indicative of vacancy ordering were observed, nor was there any reflection broadening suggesting any structural distortion. Typical fitted diffraction patterns collected throughout the heating/cooling cycle under hydrogen flow are displayed for $Ln_2Sr_2CrNiO_{8-\delta}$ in Fig. 2, S5 and S6†; the impurity detected for Ln = La was modelled as SrO once the sample had been heated above 650 °C, in agreement with the reported decomposition temperature of $SrCO_3$.[29] When the reduced samples were left at ~700 °C under hydrogen, no further change in the peak intensity occurred, and no additional

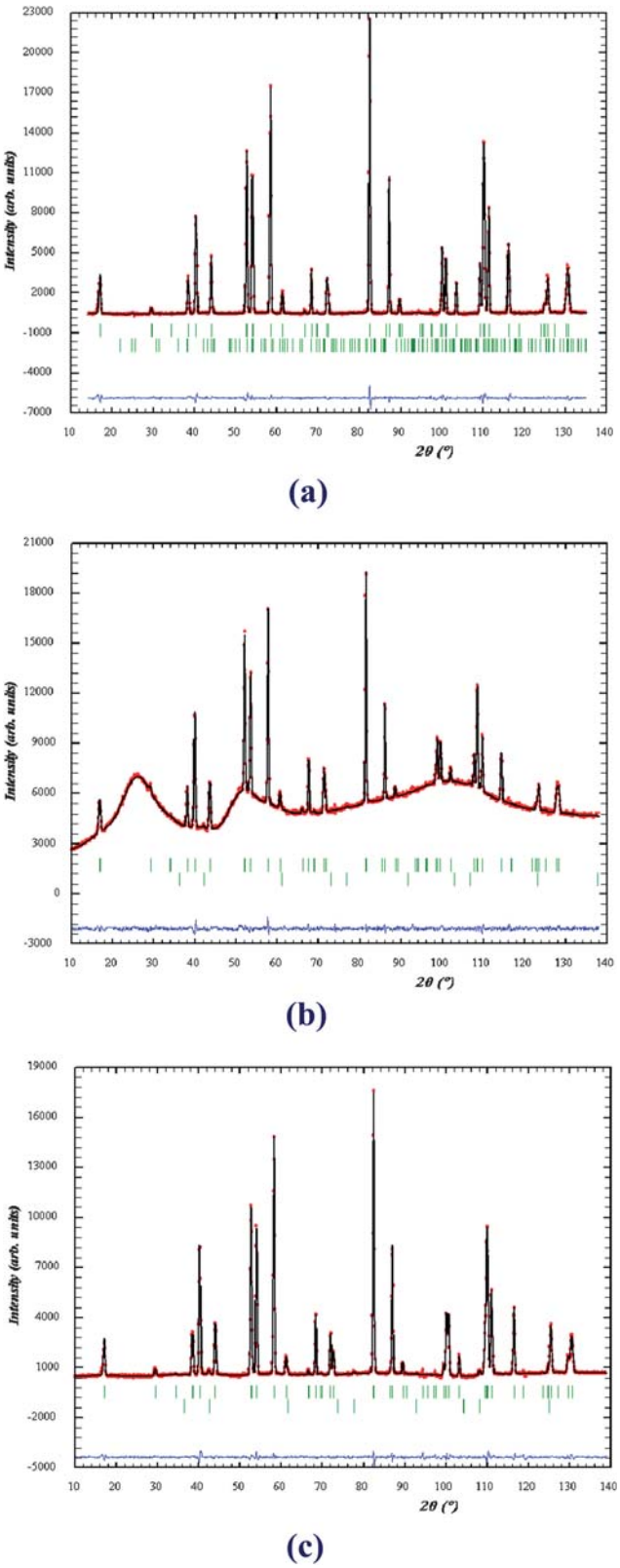

Fig. 2 Rietveld refinements of the neutron powder diffraction patterns of $La_2Sr_2CrNiO_{8-\delta}$: (a) at 20 °C before hydrogen reduction, (b) at 700 °C after reduction, (c) at 60 °C after reduction. The lower set of tick marks correspond to $SrCO_3$ impurity at 20 °C and SrO impurity at 700 and 60 °C. The data in (b) are presented without background subtraction in order to show the undulating background level attributable to diffuse scattering from the quartz tube.

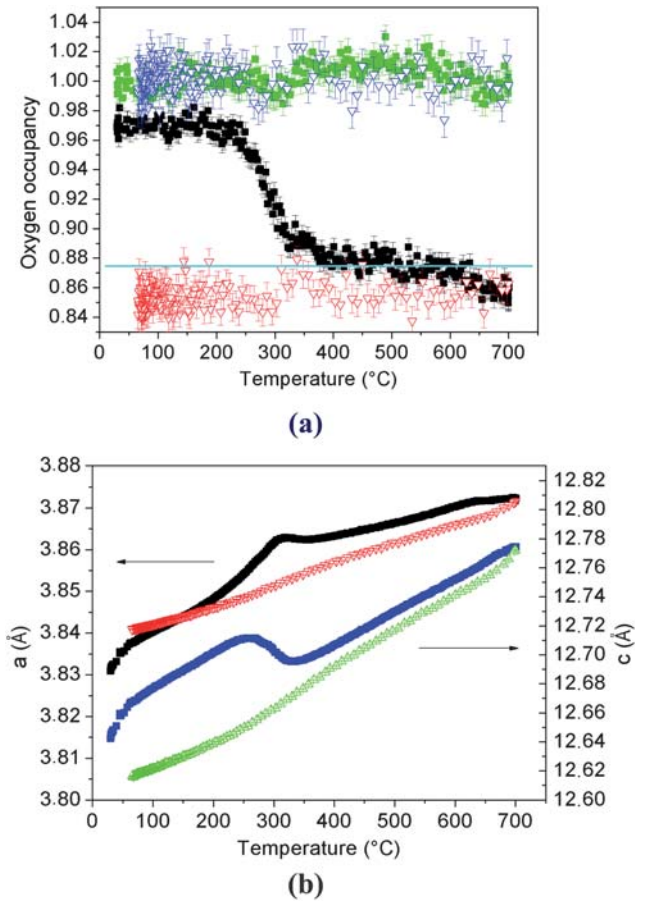

Fig. 3 (a) Occupancy factor of oxygen sites in $La_2Sr_2CrNiO_{8-\delta}$ as a function of temperature under hydrogen flow. Green and black squares represent the occupancy of O1 (axial) and O2 (equatorial) sites during heating; blue and red triangles represent O1 and O2 on cooling. The blue line corresponds to the Ni(II) composition. (b) Temperature dependence of the unit cell parameters of $La_2Sr_2CrNiO_{8-\delta}$ under hydrogen flow. Data collected on heating are represented by blue and black squares; data collected on cooling by red and green triangles.

diffraction lines attributable to impurity phases were detected, in agreement with the *ex situ* XRD study performed after heating the as-prepared samples at ~700 °C for 8 h under 5% H_2 (Fig. S2–S4†). Sequential Rietveld refinements of the NPD diagrams collected throughout the heating/cooling cycle under hydrogen indicated that reduction occurs in the temperature range 200–700 °C and involves oxygen deintercalation from the O2 site in the $(Cr/Ni)O_2$ layers; the occupation of the axial site (O1) remains unchanged, as shown in Fig. 3 and S7†. Two reduction steps are observed for $La_2Sr_2CrNiO_{8-\delta}$; the first involves deintercalation of 0.39 oxygen per f.u. from $La_2Sr_2CrNiO_{7.87(2)}$ to form $La_2Sr_2CrNiO_{7.48(2)}$, a Ni(II)-composition. The change in the oxygen occupancy matches the weight decrease observed in TGA (0.88 wt%) (Fig. 1) within experimental error and the subsequent plateau observed in both NPD and TGA (Fig. 1 and 3) confirms the existence of a thermodynamically metastable intermediate Ni(II)-composition. Raising the temperature in the NPD experiment to ~650 °C induces further loss of 0.08 oxygen per f.u. from the equatorial layers, resulting in the formation of $La_2Sr_2CrNiO_{7.40(2)}$, a mixed Ni(II,I)-composition which remains stable up to the highest temperature reached in the neutron experiment (~700 °C). The oxygen loss involved in the second reduction step, as determined by neutron diffraction, corresponds to a weight decrease smaller than that observed in the second weight loss in the TGA curve (0.19/0.60 wt%). This difference can be attributed to the contribution from the $SrCO_3$ impurity. The structural parameters and bond lengths refined for $La_2Sr_2CrNiO_{8-\delta}$ throughout the heating cycle are shown in Fig. 4 and listed in Tables 2 and 3.

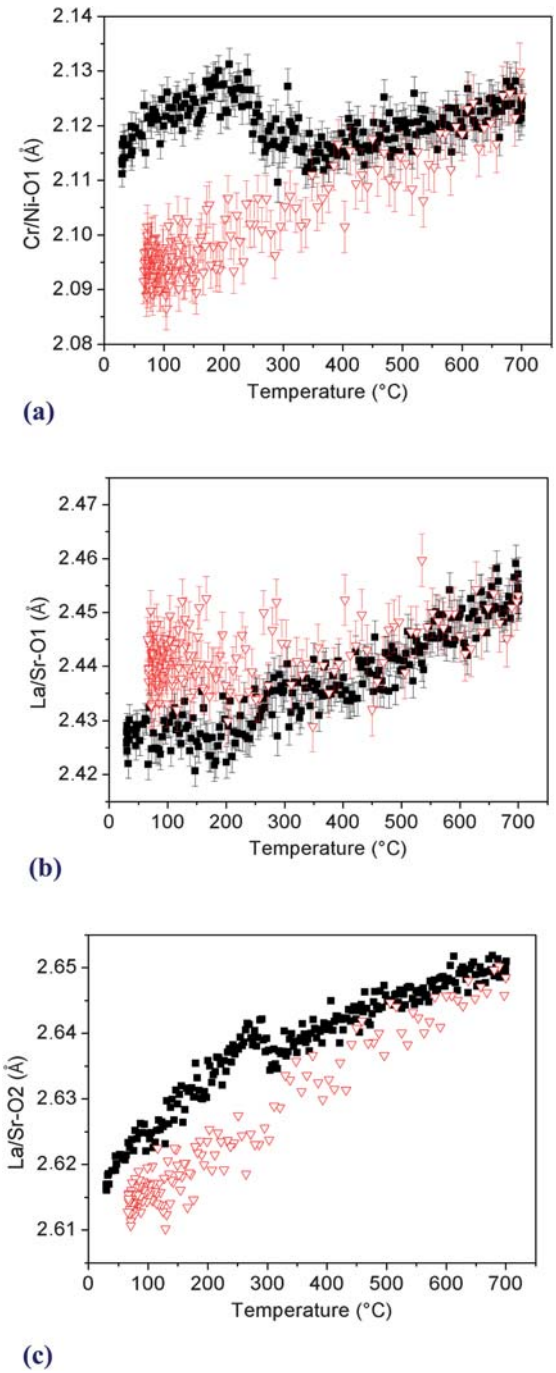

Fig. 4 Temperature dependence of the (a) Cr/Ni–O1, (b) La/Sr–O1 (along the *c*-axis) and (c) La/Sr–O2 bond lengths of $La_2Sr_2CrNiO_{8-\delta}$ under hydrogen flow. Squares (triangles) represent data collected on heating (cooling).

Table 2 Structural parameters of $La_2Sr_2CrNiO_{8-\delta}$ derived from neutron diffraction data[a]

		Before reduction/20 °C	After reduction/700 °C	After reduction/60 °C	After reoxidation/53 °C
a/Å		3.8297	3.8691(1)	3.8391(1)	3.8329(1)
c/Å		12.6345	12.7636(2)	12.6117(1)	12.6288(2)
V/Å^3		185.31	191.07(1)	185.88(1)	185.53(1)
δ		0.13(2)	0.61(3)	0.60(2)	0.13(4)
R_{wp}		4.88	8.60	4.82	11.8
R_p		8.04	17.0	9.05	22.2
χ^2		4.60	1.71	3.14	1.11
La/Sr	z	0.3592(2)	0.3582(2)	0.3592(1)	0.3592(3)
	β_{11}	0.0102(6)	0.037(1)	0.0188(6)	0.012(2)
	β_{33}	0.00053(9)	0.0023(2)	0.0011(1)	0.0012(3)
Cr/Ni	β_{11}	0.0009(8)	0.020(2)	0.0079(8)	0.004(2)
	β_{33}	0.0012(2)	0.0030(3)	0.0011(2)	0.0005(4)
O1	Occupancy	1.004(5)	1.007(7)	1.000(5)	1.01(1)
	z	0.1672(2)	0.1669(3)	0.1662(2)	0.1664(3)
	β_{11}	0.0227(8)	0.066(2)	0.0336(8)	0.027(2)
	β_{33}	0.0018(2)	0.0043(4)	0.0022(2)	0.0011(4)
O2	Occupancy	0.968(4)	0.847(6)	0.849(4)	0.968(9)
	β_{11}	0.016(2)	0.057(3)	0.035(2)	0.022(3)
	β_{22}	0.001(2)	0.014(3)	0.004(2)	0.004(3)
	β_{33}	0.0015(2)	0.0038(3)	0.0019(2)	0.0015(3)

[a] Space group *I*4/*mmm*. La/Sr on 00z, Cr/Ni on 000, O1 on 00z, O2 on 0½0.

Table 3 Selected bond lengths (Å) in $La_2Sr_2CrNiO_{8-\delta}$

	Before reduction/20 °C	After reduction/700 °C	After reduction/60 °C	After reoxidation/53 °C
La/Sr–O1	2.427(2)	2.448(4)	2.439(2)	2.426(10)
	2.730(1) × 4	2.756(1) × 4	2.735(1) × 4	2.730(2) × 4
La/Sr–O2	2.617(1) × 4	2.651(2) × 4	2.616(1) × 4	2.626(4) × 4
Ni/Cr–O1	2.113(2) × 2	2.127(3) × 2	2.095(2) × 2	2.099(8) × 2
Ni/Cr–O2	1.916(1) × 4	1.936(1) × 4	1.921(1) × 4	1.918(1) × 4

In contrast to $La_2Sr_2CrNiO_{7.87(2)}$, the evolution of the oxygen occupancies and lattice parameters of $Nd_2Sr_2CrNiO_{7.84(3)}$ and $Nd_{2.25}Sr_{1.75}CrNiO_{7.85(2)}$ under hydrogen indicates that these materials lose oxygen within a single reduction step which occurs between 200 and 400 °C (Fig. S7 and S8†). The oxygen release in $Nd_2Sr_2CrNiO_{7.84(3)}$ (0.46 ions per f.u.) and $Nd_{2.25}Sr_{1.75}CrNiO_{7.85(2)}$ (0.36 ions per f.u.) results in the mixed Ni(I,II)-compositions, $Nd_2Sr_2CrNiO_{7.38(2)}$ and $Nd_{2.25}Sr_{1.75}CrNiO_{7.49(4)}$, in agreement with the results of TGA. The refined structural parameters and bond lengths of the neodymium-containing samples are listed in Tables 4–7.

The reduction of the three materials studied can be monitored by the thermal evolution of the lattice parameters which shows an abrupt change of gradient at the onset of each reduction step. The linear evolution upon heating beyond the reduction temperature and on cooling down to room temperature is consistent with the absence of any phase transition in the reduced material (Fig. 3 and S8†). The average thermal expansion coefficient of the reduced lanthanum-containing sample ($\sim$11.9 × 10^{-6} K^{-1}) is similar to that of YSZ (10.3 × 10^{-6} K^{-1} in both air and H_2), the most commonly used electrolyte in a SOFC[36,37] suggesting that there would be good compatibility between these materials under fuel-cell operating conditions.

Comparison of the stoichiometries, as determined by TGA, of the reduced compounds at 400 °C ($La_2Sr_2CrNiO_{7.50(5)}$, $Nd_2Sr_2CrNiO_{7.40(5)}$ and $Nd_{2.25}Sr_{1.75}CrNiO_{7.55(5)}$) indicates that the concentration of the oxygen vacancies introduced at this temperature can be increased *via* the incorporation of a small lanthanide (Nd *vs.* La) or *via* Sr-doping within the Nd-series. These observations are consistent with results obtained on cuprates $Ln_2CuO_{4-\delta}$; $\delta = 1/3$ for La and 1/2 for Nd[38] and on reduced nickelates $La_{1.6}Sr_{0.4}NiO_{3.47}$ and $LaSrNiO_{3.1}$.[39,40] No intermediate phase containing only the Ni(II) oxidation state could be stabilized during our *in situ* neutron study of the two Nd-compositions, probably because of the fast kinetics favored by the experimental configuration used during the reduction of these samples, that is with the reducing gas passing through the sample (in contrast to the reduction of $La_2Sr_2CrNiO_{8-\delta}$ where the reducing gas was flowing over the sample). However, it is interesting that the lowest oxidation state attained by nickel is approximately the same (1.8) in $Nd_2Sr_2CrNiO_{7.38}$, $Nd_{2.25}Sr_{1.75}CrNiO_{7.49}$ and $La_2Sr_2CrNiO_{7.40}$.

The oxide-ion vacancies created in these materials remain disordered and confined to the equatorial layers of the K_2NiF_4 structure at all temperatures in agreement with results obtained previously on reduced manganates,[41] but in contrast to the behaviour of $NdSrCuO_{3.56}$ wherein the oxide vacancies are distributed between axial and equatorial positions.[42] Attempts to refine models with ordered oxide vacancies in larger unit cells in a manner similar to $Ca_2MnO_{3.5}$[43] were unsuccessful. No evidence of symmetry lowering on reduction was observed; thus ruling out differential occupancy of the (0,0.5,0) and (0.5,0,0) sites, as was

Table 4 Structural parameters of $Nd_2Sr_2CrNiO_{8-\delta}$ derived from neutron diffraction data

		Before reduction/20 °C	After reduction/710 °C	After reduction/90 °C	After reoxidation/81 °C
a/Å		3.79689(4)	3.83217(6)	3.80584(3)	3.80182(7)
c/Å		12.4637(2)	12.6206(2)	12.5116(1)	12.4729(3)
V/Å^3		179.68(1)	185.34(1)	180.46(1)	180.28(1)
δ		0.16(3)	0.60(3)	0.62(3)	0.04(6)
R_{wp}		7.59	10.3	10.5	17.1
R_p		17.2	24.3	24.0	38.1
χ^2		2.87	2.11	0.77	2.79
Nd/Sr	z	0.3581(2)	0.3571(3)	0.3578(3)	0.3575(4)
	β_{11}	0.0124(9)	0.043(2)	0.022(2)	0.012(2)
	β_{33}	0.0006(2)	0.0030(3)	0.0007(3)	0.0006(4)
Cr/Ni	β_{11}	0.006(2)	0.029(2)	0.015(2)	0.008(3)
	β_{33}	0.0004(3)	0.0028(4)	0.0004(4)	0.0006(5)
O1	Occupancy	1.002(8)	0.998(9)	1.00(1)	1.03(2)
	z	0.1678(3)	0.1672(3)	0.1670(4)	0.1684(5)
	β_{11}	0.033(2)	0.082(2)	0.044(2)	0.039(3)
	β_{33}	0.0025(3)	0.0039(5)	0.0031(4)	0.0028(6)
O2	Occupancy	0.960(6)	0.850(7)	0.845(8)	1.01(1)
	β_{11}	0.016(3)	0.077(4)	0.048(4)	0.016(5)
	β_{22}	0.010(3)	0.024(4)	0.006(4)	0.004(5)
	β_{33}	0.0022(3)	0.0040(4)	0.0020(3)	0.0027(5)

Table 5 Selected bond lengths (Å) in $Nd_2Sr_2CrNiO_{8-\delta}$

	Before reduction/20 °C	After reduction/710 °C	After reduction/90 °C	After reoxidation/80 °C
Nd/Sr–O1	2.374(3)	2.400(5)	2.379(4)	2.363(8)
	2.706(1) × 4	2.729(1) × 4	2.711(1) × 4	2.711(1) × 4
Nd/Sr–O2	2.596(2) × 4	2.632(2) × 4	2.602(2) × 4	2.599(3) × 4
Ni/Cr–O1	2.093(2) × 2	2.112(4) × 2	2.082(4) × 2	2.107(6) × 2
Ni/Cr–O2	1.900(1) × 4	1.917(1) × 4	1.904(1) × 4	1.902(1) × 4

Table 6 Structural parameters of $Nd_{2.25}Sr_{1.75}CrNiO_{8-\delta}$ derived from neutron diffraction data

		Before reduction/20 °C	After reduction/450 °C	After reduction/80 °C
a/Å		3.80321(3)	3.83572(3)	3.81589(7)
c/Å		12.4202(1)	12.5116(1)	12.4227(3)
V/Å^3		179.65(1)	184.08(1)	180.89(1)
δ		0.15(2)	0.46(2)	0.51(4)
R_{wp}		4.84	5.34	13.1
R_p		7.72	9.82	25.3
χ^2		7.04	3.20	1.09
Nd/Sr	z	0.3584(1)	0.3580(1)	0.3580(3)
	β_{11}	0.0117(6)	0.0294(7)	0.021(2)
	β_{33}	0.0005(1)	0.0017(2)	0.0004(3)
Cr/Ni	β_{11}	0.0072(8)	0.0197(8)	0.012(2)
	β_{33}	0.0006(2)	0.0024(2)	0.0007(4)
O1	Occupancy	1.008(5)	1.006(5)	1.01(2)
	z	0.1686(2)	0.1683(2)	0.1682(4)
	β_{11}	0.0353(8)	0.069(1)	0.048(2)
	β_{33}	0.0023(2)	0.0035(2)	0.0045(5)
O2	Occupancy	0.964(4)	0.886(4)	0.876(9)
	β_{11}	0.014(2)	0.055(2)	0.028(4)
	β_{22}	0.008(2)	0.017(2)	0.015(4)
	β_{33}	0.0017(2)	0.0033(2)	0.0014(3)

observed in structurally related nickel-based oxides[39,40] resulting in an orthorhombic distortion to space group *Immm*. Our refinements also rule out a cooperative rotation of the (Cr/Ni)O_6 octahedra around the z-axis, a behavior commonly observed in isostructural Co-containing materials such as $LaSrCo_{0.5}Fe_{0.5}O_{3.75}$[8] which has an oxygen content similar to that of our reduced materials. The reduced samples are stable in air at room temperature. However, heating in an oxidizing atmosphere (air, O_2) induces oxygen intercalation into the equatorial position (O2) with retention of the *I*4/*mmm* space group as demonstrated by the Rietveld refinements (Fig. 5 and Tables 2 and 4). The evolution of the oxygen occupancies and cell parameters, displayed in Fig. 6 and S9†, is consistent with the reoxidative behavior observed by TGA under flowing O_2; the reduced materials gain mass rapidly at ~400 °C (Fig. 1). The reversibility of the redox reaction was not predictable from a structural point of view because of the availability of both equatorial and interstitial vacant sites in the reduced materials and the possibility that equatorial vacancies might coexist with interstitial oxygen atoms.[44,45] The refined oxygen occupancies in the reoxidized materials show full occupancy of the axial position (O1) together with a variable level of deficiency at the equatorial site (O2); the La-containing composition returned to the stoichiometry of the as-prepared sample, whereas the O2 lattice of $Nd_2Sr_2CrNiO_{8-\delta}$ was free of vacancies. The latter result is in agreement with that obtained by iodometry, whereas the former is not. This is likely to be attributable to the differences in the experimental conditions used to study the reoxidation process by neutron diffraction. In addition to the differences in the configuration of the gas-flow system described above, $Nd_2Sr_2CrNiO_{8-\delta}$ was held in air at ~550 °C for more than 7 h whereas $La_2Sr_2CrNiO_{8-\delta}$ was held for only 1 h at 500 °C. Thus, it is reasonable to expect that a greater degree of reoxidation might occur in the case of the Nd-

Table 7 Selected bond lengths (Å) in $Nd_{2.25}Sr_{1.75}CrNiO_{8-\delta}$

	Before reduction/20 °C	After reduction/450 °C	After reduction/80 °C
Nd/Sr–O1	2.359(2)	2.376(2)	2.359(6)
	2.712(1) × 4	2.732(1) × 4	2.720(1) × 4
Nd/Sr–O2	2.592(1) × 4	2.615(1) × 4	2.600(2) × 4
Ni/Cr–O1	2.096(2) × 2	2.107(2) × 2	2.091(5) × 2
Ni/Cr–O2	1.903(1) × 4	1.917(1) × 4	1.909(1) × 4

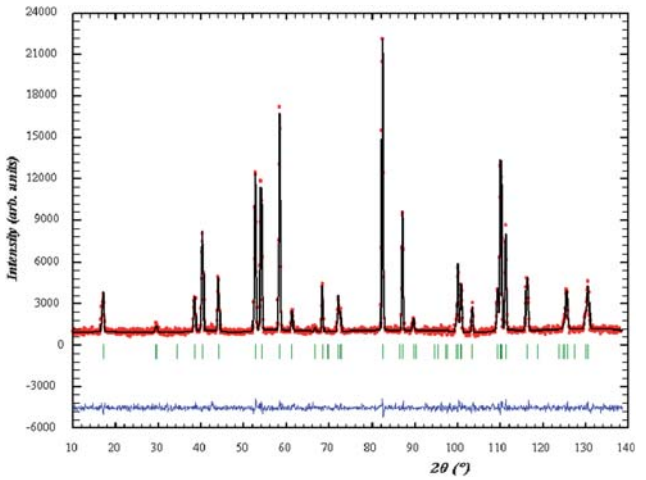

Fig. 5 Single-phase Rietveld refinement of the neutron powder diffraction pattern of $La_2Sr_2CrNiO_{8-\delta}$ at 53 °C after reoxidation (heating/cooling cycle of the reduced material under air flow).

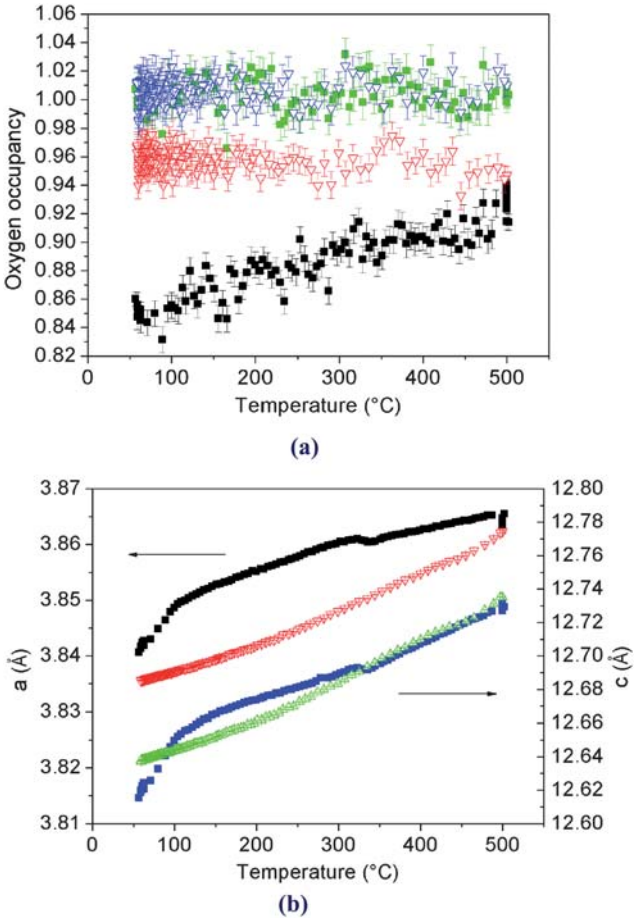

Fig. 6 (a) Occupancy factor of oxygen sites in $La_2Sr_2CrNiO_{8-\delta}$ as a function of temperature under oxidizing conditions after reduction. Green and black squares represent the occupancy of O1 (axial) and O2 (equatorial) sites during heating; blue and red triangles represent O1 and O2 during cooling. (b) Temperature dependence of the unit cell parameters of $La_2Sr_2CrNiO_{8-\delta}$ under oxidizing conditions. Squares (triangles) represent data collected on heating (cooling).

containing sample. It is clear from Fig. 6a that the occupancy factor of the equatorial oxygen, O2, in $La_2Sr_2CrNiO_{8-\delta}$ did not reach a constant value during the *in situ* reoxidation experiment.

The shift in the temperature range of the reduction reaction as determined by NPD and TGA can be attributed to the temperature calibration and the difference in the configuration of the sample environment. In particular, the position of the control thermocouple in the neutron experiment was about 1 cm above the illuminated sample (*i.e.* 4 cm above the centre of the neutron beam). Moreover, differences in the mass of sample used in the two experiments (~500 mg in a quartz tube of 10 mm diameter, compared to ~100 mg in a quartz crucible of 2 mm diameter hanging from a quartz rod), the gas flow rates and the heating rates are all known to affect the kinetics and thermodynamics of the reduction reaction.[46] The problem of ensuring self-consistency between diffraction data and TGA data will only be overcome when a dual-purpose instrument has been developed that allows both to be collected simultaneously *in situ*.

Hydrogen reduction did not result in a pure Ni(I) composition in any of the systems studied. When our samples were left in 5% H_2 at ~700 °C for 30 min, NPD ascertained that reduction did not proceed further and that no sample decomposition occurred. The excellent thermal stability of our oxygen-deficient oxides under strong reducing conditions contrasts with the behavior of the 3D perovskites, $LaCr_{1-x}Ni_xO_{3-\delta}$ which leach Ni-metal under a reducing atmosphere even when a Cr : Ni ratio of 9 : 1 is used in an attempt to retain structural stability.[47] In view of these results, one might conclude that the layered RP compounds are more stable in reducing conditions than the analogous perovskites. This is particularly true for K_2NiF_4-like phases some of which are "reduction products" of the 3D perovskites.[48,49] The Ni(I) oxidation state is rather rare in oxides, although $LaNiO_2$[50] and $YSr_5Ni_3O_8$[51] have been obtained by low temperature (<300 °C) hydrogen reduction of Ni(III) ternary oxides. Millburn and Rosseinsky have reported the existence of the pure Ni(I) composition, $La_2Sr_2CrNiO_{7.0}$, obtained by hydrogen reduction of $La_2Sr_2CrNiO_{8.0}$.[34] The oxygen content of their sample was determined only by TGA under hydrogen; no neutron diffraction study was carried out. However, the volume change shown by their sample on reduction (0.56%) is larger than that shown by our sample (0.41%), consistent with a higher degree of reduction. Refinement of the crystal structure of their reduced material, using XRD data collected at room temperature, showed that the vacancies exclusively form in the perovskite layers $(Cr/Ni)O_x$, and order preferentially along one axis such that the structure distorts to orthorhombic *Fmmm* symmetry.[34] A possible reason for the higher degree of reduction observed by Millburn and Rosseinsky might stem from their use of hydrogen gas that had

been predried over activated molecular sieves; our gas was not dried. The use of slightly wet gas creates a higher oxygen partial pressure over the sample,[52] which can result in a lower degree of reduction. The adoption of a symmetry consistent with vacancy ordering suggests that some degree of Cr/Ni ordering is present in $La_2Sr_2CrNiO_{7.0}$ because Cr^{3+} is unlikely to be found in a coordination geometry other than octahedral; the vacancies would be expected to occur preferentially in the coordination shell of Ni^+. The X-ray data available to Millburn and Rosseinsky did not allow them to identify Cr/Ni ordering, and the ordering of the anion vacancies was deduced from the symmetry of the reduced material. It would certainly be interesting to study the fully reduced material by neutron diffraction. However, even this technique might not identify the presence of cation ordering. Indeed, no ordering was detected[53] by neutron diffraction in La_4LiMnO_8 and $La_3SrLiMnO_8$, although ^6Li MAS NMR showed clearly that it was present in both cases. High-resolution electron microscopy subsequently showed that Li/Mn ordering is present in each perovskite-like sheet, but that the sheets are stacked in a random manner along [001]. It is possible that the $Ln_2Sr_2CrNiO_{8-\delta}$ compositions contain similar defects at the microstructural level; this would be consistent with the anisotropic peak width observed in our X-ray diffraction patterns (Fig. S10†).

The composition of our reduced samples at ~400 °C has been established in the present *in situ* study as being close to $Ln_2Sr_2CrNiO_{7.5}$ (*Ln* = La, Nd). This stoichiometry corresponds to the removal of 0.5 oxygen per Cr/Ni octahedron. In order to satisfy the strong preference of Cr^{3+} for an octahedral environment, it seems likely that the anion vacancies are shared by pairs of Ni^{2+} cations. The oxygen deficiency would then be accommodated by a mixture of 6-coordinate Cr^{3+} and 5-coordinate square-pyramidal Ni^{2+}. It has been suggested that vacancy ordering, accompanied by a reduction in symmetry, can occur in these $n = 1$ systems,[34,39,40] but we observe no direct evidence for this. Such an ordering might be accompanied by an ordering of the Cr^{3+} and Ni^{2+} ions in distinct layers, at least on a short length scale. This would be driven by the significant difference in cationic radii as well as by the different coordination preferences. However, we emphasise that there is no evidence for cation ordering in our neutron diffraction data. Detailed HRTEM studies are in progress to investigate whether such ordering is present in small microdomains.

Comparison of the unit cell parameters before reduction with those determined after reduction and subsequent cooling reveals that the oxygen loss is accompanied by an increase in the unit cell size in the *xy* plane and a decrease along *z*; the volume of the unit cell shows a net increase (Tables 2, 4 and 6). The volume expansion of the unit cell depends on the cation size at the *A*-site; ΔV = 0.34, 0.43 and 0.69% for $La_2Sr_2CrNiO_{8-\delta}$, $Nd_2Sr_2CrNiO_{8-\delta}$ and $Nd_{2.25}Sr_{1.75}CrNiO_{8-\delta}$, respectively. It is quite surprising that $Nd_{2.25}Sr_{1.75}CrNiO_{8-\delta}$, which shows the lowest oxygen loss, exhibits the highest volume expansion upon reduction. This behavior is consistent with that of the Ln_2CuO_4 cuprates (*Ln* = La, Nd) where the less reduced compound, $La_2CuO_{4-\delta}$ ($\delta = 1/3$) exhibits a larger cell-volume expansion than $Nd_2CuO_{4-\delta}$ ($\delta = 1/2$); 6%/1%.[38]

As a result of the faster heating rate used, fewer diffraction patterns were collected below the transition temperature in the case of the Nd compositions than in the case of $La_2Sr_2CrNiO_{8-\delta}$. Thus, the relatively small changes in the low-temperature bond lengths that occur as a result of the reduction process can be discussed with more confidence for the $La_2Sr_2CrNiO_{8-\delta}$ system. The Cr/Ni–O2 distance, which is directly related to the in-plane unit-cell parameter, increases despite the introduction of vacancies onto the O2 site. This increase stems from the presence of an additional electron in the antibonding $d_{x^2-y^2}$ orbital of the Ni cations. A striking feature is the contraction of the Cr/Ni–O1 bond along the *z*-axis upon reduction (Fig. 4 and Table 3) suggesting a low spin d^7 configuration for Ni(III) in the as-prepared material and a decrease in the Jahn–Teller distortion upon reduction. Such behavior is further confirmation that reduction of Ni(III) leads predominantly to Ni(II) rather than Ni(I) because Ni(I) is also a Jahn–Teller ion. An increase of the *M*–O1 bond following reduction has been observed in Co-containing oxides when low-spin Co^{3+} reduces to high-spin Co^{2+},[7,8] although this change is a consequence of the increase in ionic size rather than a consequence of a Jahn–Teller distortion.

Despite the expansion of the shortest La/Sr–O1 bond (along the *z*-axis), the contraction of the Cr/Ni–O1 bond (Fig. 4), which relieves the strain on the interlayer space, results in a reduction of the *c* parameter (Table 2). Consequently, the bidimensional character of the structure is lower in the reduced materials. Reduction beyond Ni(II) requires the introduction of a second electron into the d_{z^2} orbital, which would be expected to lengthen the Cr/Ni–O1 bond and hence to exert stress on the rock-salt layers. The tendency of the $3d^9$ Ni(I) cation to undergo a Jahn–Teller distortion would magnify this effect. This induced stress might determine, in part, the level of reduction that can be achieved. The expansion of the La/Sr–O1 bond is balanced by a contraction of the La/Sr–O2 bond length (Fig. 4). Thus, the polyhedron around the La/Sr cation gets more symmetrical as the Ni(III) content decreases. The less extensive data available on the bond lengths in $Nd_2Sr_2CrNiO_{8-\delta}$ and $Nd_{2.25}Sr_{1.75}CrNiO_{8-\delta}$ are shown in Fig. S11 and S12†. Although the contraction of the Cr/Ni–O1 bond after reduction is apparent, it is difficult to draw reliable conclusions concerning the bond lengths around the Nd/Sr site.

The displacement parameters of some of the atoms in $La_2Sr_2CrNiO_{8-\delta}$ at room temperature before reduction show significant anisotropy. In particular, in the case of the equatorial oxide ion O2, β_{11} is much larger than β_{22} (Fig. 7). This suggests that the disorder on the transition-metal sublattice is accommodated by displacements of the anion perpendicular to, rather than along, the interatomic vector. The transition-metal cations themselves are displaced along [001], rather than within the perovskite sheets, but the La/Sr cations have a slightly larger displacement within the layers. A similar but less marked anisotropy was found at the O2 and *Ln*/Sr sites before reduction in the other compositions studied, both in this work and previously.[11] It is interesting to note that this anisotropy was not observed in a high-resolution neutron-diffraction study of Millburn and Rosseinsky's sample of $Ln_2Sr_2CrNiO_8$.[54] This might reflect a difference in the degree of local Cr/Ni ordering in the two samples. The anisotropy associated with the displacement parameters of O2 in $La_2Sr_2CrNiO_{8-\delta}$ persisted throughout the heating/cooling cycle under hydrogen, as is shown by the thermal ellipsoids in Fig. 7b and c. It was more apparent in the reduced

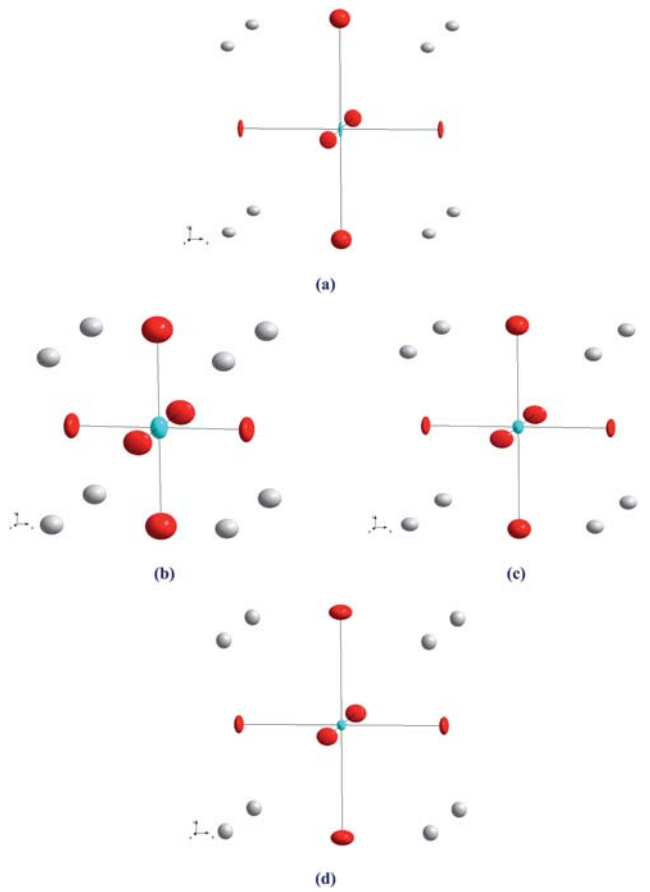

Fig. 7 Thermal ellipsoids for La/Sr (white), Cr/Ni (cyan) and O (red) in $La_2Sr_2CrNiO_{8-\delta}$: (a) at 20 °C before reduction, (b) at 700 °C after reduction, (c) at 60 °C after reduction and subsequent cooling, (d) at 53 °C after reoxidation at up to ~500 °C in air.

forms of the other compositions, both at high temperature and on subsequent cooling to below 100 °C (Tables 4 and 6). The anisotropy associated with the transition-metal site of $La_2Sr_2CrNiO_{8-\delta}$ at low temperature was greatly reduced following oxygen loss, suggesting that the introduction of vacancies in the *xy* plane relieves the structural strain. For all atoms, the low-temperature displacement parameters after reduction were generally higher than those prior to reduction, reflecting the increased disorder in the structure (Tables 2, 4 and 6). Retention of *I*4/*mmm* symmetry (*i.e.* the absence of vacancy ordering over the neutron-diffraction length scale) throughout the reduction reaction might be due to the low concentration of oxygen vacancies introduced. Retention of *I*4/*mmm* symmetry has, however, been observed in many reduced RP oxides, even when higher oxygen vacancy concentrations were introduced.[7]

Our *in situ* experiments established that oxygen was removed from the equatorial positions of the K_2NiF_4-type oxides and that no redistribution of the remaining oxygen between the different sites (axial, equatorial and interstitial) occurs during the reduction reaction or when cooling the samples to room temperature. Such behavior was not entirely predictable because the oxygen release from the different sites might vary with the reduction level. Indeed, Hayward has shown that at a low level of reduction, oxide ions are removed from both the equatorial and axial oxygen sites of the $n = 2$ Ruddlesden–Popper phase $YSr_2Mn_2O_{7.0}$, yielding $YSr_2Mn_2O_{6.0}$. However, upon further reduction of $YSr_2Mn_2O_{7.0}$ to $YSr_2Mn_2O_{5.5}$, all the oxygen vacancies were found to occur in the MnO_2 sheets, leaving the axial sites fully occupied.[55] Any oxygen diffusion in the $Ln_2Sr_2CrNiO_{8-\delta}$ compounds should occur through a vacancy mechanism within the equatorial layers, with the oxygen conductivity increasing with increasing vacancy concentration.

In an attempt to understand why oxygen was lost only from the O2 site, bond valence calculations were performed.[56,57] A departure from the ideal BVS sum is an indication of stress in the structure. The valences calculated for the axial and equatorial oxygens in $La_2Sr_2CrNiO_{8-\delta}$ from the bond distances listed in Table 3 are 1.63 and 2.25. These values indicate that the O1 and O2 atoms are respectively underbonded (tensile stress) and overbonded (compressive stress). These bond strains are created by a size mismatch between the rock-salt and perovskite layers, as observed in many K_2NiF_4-type oxides.[58] Our results show that relatively small changes in the bond lengths and BVS values accompany the creation of anion vacancies during the reduction process. Calculations which should enable us to understand the reason for the loss of oxide ions from the equatorial, rather than axial, sites are in progress. These calculations might also be able to predict the relative thermodynamic stability of $n = 1$ RP structures in which the anion vacancies are ordered and disordered.

Conclusion

High quality neutron diffraction data have been collected *in situ* under hot, flowing hydrogen in order to determine the reductive behavior of potential anode materials from both a structural and a chemical point of view. The results show that hydrogen reduction of the K_2NiF_4-type materials, $Ln_2Sr_2CrNiO_{8-\delta}$, proceeds *via* oxygen deintercalation from the (Cr/Ni)O_2 layers; the occupancy of the oxygen site within the rocksalt (*Ln*/Sr)O layers remained unchanged throughout the heating/cooling cycle under H_2-gas. Reduction of the $La_2Sr_2CrNiO_{8-\delta}$ material led to an intermediate Ni(II) composition, $La_2Sr_2CrNiO_{7.5}$ *en route* to a mixed valent Ni(II,I) compound, $La_2Sr_2CrNiO_{7.4}$. Our neutron data show no evidence for any pure Ni(I) composition, in contrast to previous results reporting the formation of $La_2Sr_2CrNiO_7$ *via* hydrogen reduction of $LaSrCr_{0.5}Ni_{0.5}O_4$. Comparison of the behaviour of the three systems studied shows that the change in the total oxygen content, as determined by NPD, upon heating the material under hydrogen gas at 400 °C can be increased by reducing the size of the lanthanide cation or by doping with Sr^{2+}. The oxygen content determined by neutron diffraction is consistent with the mass loss observed by TGA. The chemical reduction was mirrored by the change in gradient of the temperature dependence of the lattice parameters.

Investigation of the high-temperature chemistry and thermodynamics of ceramic materials under both reducing and oxidizing atmospheres is necessary in order to determine their stability and understand the degradation and corrosion processes which they might undergo under fuel-cell working conditions. The work described above demonstrates that these $n = 1$ RP phases, $Ln_{3-x}Sr_{1+x}CrNiO_{8-\delta}$ possess remarkable structural stability in strongly reducing conditions, particularly in

comparison to perovskites having the same cations on the six-coordinate sites. The absence of significant structural change would help to reduce redox shock on fuel-cell cycling. Regardless of whether these materials find a use in high-temperature ionic devices, this demonstration that subtle structural information can be gathered *in situ* in extreme environments opens up the possibility of studying many important systems provided that suitable gas-handling equipment is available in neutron research centres. An oxide material in a device might undergo a structural phase change on cooling from the operating temperature to ambient conditions.[59] It is also possible that a change in the relative occupation factors of the available anion sites within a single phase (O1, O2 and interstitial in the case of an $n = 1$ RP material) might occur as a result of anisotropic contraction of the lattice on cooling through a temperature regime where anion diffusion is still possible; this may or may not result in an ordering of anion vacancies. In these cases a subsequent structural study at room temperature would not give a true picture of the structure and dynamics of the material under high-temperature working conditions. Neither would such a study reveal the existence of transitory intermediates that might form between room temperature and the working temperature, nor would it allow the order of any phase transition to be established through the observation, or otherwise, of hysteresis in the structural changes. The value of high-temperature neutron diffraction in establishing diffusion pathways in oxide-ion conductors has already been demonstrated by Yashima *et al.*[60] and the insight offered by such studies could be enhanced if they were to be carried out under a wide range of controlled gas pressures and atmospheres (H_2, H_2/H_2O, O_2), thus allowing the oxygen content of the conductor to be varied in a systematic manner. In the case of electrocatalytic reactions occurring at the electrodes of a SOFC, *in situ* studies under realistic working conditions would reveal how the catalytic activity depends on composition, temperature and structure, thus making the process of electrocatalyst development less empirical. Extension of the method to include *in situ* studies of fuel-cell components, for example an electrolyte–electrode unit, would generate valuable information on the thermodynamics, mechanism and kinetics of any degradation process and would thus guide the design, synthesis and fabrication of improved components. Only by performing these experiments *in situ*, that is by continuously monitoring the material as a function of temperature and gas atmosphere, can we unambiguously establish the detailed crystal structure and composition under working conditions and hence learn how to improve the performance of the material under these conditions.

Acknowledgements

We are very grateful to J. Torregrossa and A. Daramsy (ILL) for assisting in the collection of the NPD data. We are grateful to S. Fourcade (ICMB, Bordeaux) for collecting some TGA data. FT thanks Région Bretagne for funding.

References

1 S. Primdahl, J. R. Hansen, L. Grahl-Madsen and P. H. Larsen, *J. Electrochem. Soc.*, 2001, **A148**, 74–81.
2 P. Holtappels, J. Bradley, J. T. S. Irvine, A. Kaiser and M. Morgensen, *J. Electrochem. Soc.*, 2001, **A148**, 923–929.
3 J. Sfeir, P. A. Buffat, P. Möckli, N. Xanthopoulos, R. Vasquez, H. J. Mathieu, J. Van Herle and K. Ravidranathan Thampi, *J. Catal.*, 2001, **202**, 229–244.
4 F. Jin, T. Endo, H. Takizawa and M. Shimada, *J. Solid State Chem.*, 1994, **113**, 138.
5 H. E. Hofer and W. E. Kock, *J. Electrochem. Soc.*, 1993, **140**, 2889.
6 A. L. Sauvet and J. T. S. Irvine, in *Proc. 5th European SOFC Forum*, ed. J. Huijsmans, European Fuel Cell Forum, Oberrohrbach, Switzerland, 2002, pp. 490–498.
7 H. El Shinawi, J. F. Marco, F. J. Berry and C. Greaves, *J. Solid State Chem.*, 2009, **182**, 2261.
8 H. El Shinawi and C. Greaves, *J. Solid State Chem.*, 2008, **181**, 2705–2712.
9 S. E. Dutton, M. Bahout, P. D. Battle, F. Tonus and V. Demange, *J. Solid State Chem.*, 2008, **181**, 2217.
10 F. Tonus and M. Bahout, unpublished results.
11 F. Tonus, M. Bahout, P. F. Henry, S. E. Dutton, T. Roisnel and P. D. Battle, *Chem. Commun.*, 2009, 2556–2558.
12 M. Karppinen, A. Fukuoka, L. Niinisto and H. Yamauchi, *Supercond. Sci. Technol.*, 1996, **9**, 121–125.
13 A. I. Vogel, *A Textbook of Quantitative Inorganic Analysis*, Longmans, London, 1961, 3rd edn.
14 H. M. Rietveld, *J. Appl. Crystallogr.*, 1969, **2**, 65.
15 J. Rodriguez-Carvajal, M. T. Fernandez-Diaz and J. L. Martinez, *J. Phys.: Condens. Matter*, 1991, **3**, 3215–3234.
16 P. Stephens, *J. Appl. Crystallogr.*, 1999, **32**, 281.
17 T. C. Hansen, P. F. Henry, H. E. Fischer, J. Torregrossa and P. Convert, *Meas. Sci. Technol.*, 2008, **19**, 034001.
18 L. B. McCusker, R. B. Von Dreele, D. E. Cox, D. Louër and P. Scardi, *J. Appl. Crystallogr.*, 1999, **32**, 36.
19 J. Rodriguez-Carvajal, *Physica B*, 1993, **192**, 55.
20 J. E. Millburn, M. A. Green, D. A. Neuwmann and M. J. Rosseinsky, *J. Solid State Chem.*, 1999, **145**, 401–420.
21 P. Lacorre, J. B. Torrance, J. Pannetier, A. I. Nazzal, P. W. Wang and T. C. Huang, *J. Solid State Chem.*, 1991, **91**, 225–237.
22 G. Demazeau, A. Marbeuf, M. Pouchard and P. Hagenmuller, *J. Solid State Chem.*, 1971, **3**, 582.
23 G. Demazeau, M. Pouchard and P. Hagenmuller, *J. Solid State Chem.*, 1976, **18**, 159–162.
24 S. H. Byeon, G. Demazeau and J. H. Choy, *Jpn. J. Appl. Phys.*, 1995, **34**, 6156.
25 D. E. Rice and D. J. Buttrey, *J. Solid State Chem.*, 1993, **105**, 197.
26 H. Tamura, A. Hayashi and Y. Ueda, *Physica C*, 1993, **216**, 83.
27 V. V. Vashook, S. P. Tolochko, I. I. Yushkevich, L. V. Makhnach, I. F. Kononyuk, H. Altenburg, J. Hauck and H. Ullmann, *Solid State Ionics*, 1998, **110**, 245.
28 A. Aguadero, M. J. Escudero, M. Perez, J. A. Alonso, V. Pomjakushim and L. Daza, *Dalton Trans.*, 2006, 4377.
29 S. A. Robbins, R. G. Rupard, B. J. Weddle, T. R. Maull and P. K. Gallagher, *Thermochim. Acta*, 1995, **269/270**, 43–49.
30 R. Sáez Puche, F. Fernández, J. Rodriguez Carvajal and J. L. Martinez, *Solid State Commun.*, 1989, **72**, 273.
31 T. Strangfeld, K. Westerholt and H. Bach, *Physica C (Amsterdam)*, 1991, **183**, 1–10.
32 A. Morales Sánchez, F. Fernández, R. Sáez Puche and F. Fernández-Martin, *J. Alloys Compd.*, 1994, **203**, 143.
33 A. Skowron, A. Petric, H. Moudallal, A. J. Jacobson and C. A. Mims, *Mater. Res. Bull.*, 1997, **32**(3), 327.
34 J. E. Millburn and M. J. Rosseinsky, *Chem. Mater.*, 1997, **9**, 511.
35 V. F. Sears, *Neutron News*, 1992, **3**, 26.
36 J. Larminie and A. Dicks, *Fuel Cells Systems Explained*, John Wiley and Sons Ltd, Wiltshire, 2nd edn, 2000, 308 pages.
37 S. P. Jiang and S. H. Chan, *J. Mater. Chem.*, 2004, **39**, 4405–4439.
38 F. C. Chou, J. H. Cho, L. L. Miller and D. C. Johnston, *Phys. Rev. B: Condens. Matter*, 1990, **42**, 6172.
39 M. Crespin, J. M. Bassat, P. Odier, P. Mouron and J. Choisnet, *J. Solid State Chem.*, 1990, **84**, 165–170.
40 M. Crespin, C. Landron, P. Odier, J. M. Bassat, P. Mouron and J. Choisnet, *J. Solid State Chem.*, 1992, **100**, 281–391.
41 L. G. Gillie, A. J. Wright, J. Hadermann, G. Van Tendeloo and C. Greaves, *J. Solid State Chem.*, 2002, **167**, 145.
42 P. H. Labbe, M. Ledesert, V. Caignaert and B. Raveau, *J. Solid State Chem.*, 1991, **91**, 362–369.

43 M. E. Leonowicz, K. R. Poeppelmeier and J. M. Longo, *J. Solid State Chem.*, 1985, **59**, 71–80.
44 V. V. Kharton, A. P. Viskup, E. N. Naumovich and F. M. B. Marques, *J. Mater. Chem.*, 1999, **9**, 2623.
45 L. Minervini, R. W. Grimes, J. Kilner and K. E. Sickafus, *J. Mater. Chem.*, 2000, **10**, 2349.
46 A. Jones and B. D. McNicol, *Temperature-Programmed Reduction for Solid Materials Characterization*, Marcel Dekker Inc., New York, 1986.
47 A. L. Sauvet and J. T. S. Irvine, *Solid State Ionics*, 2004, **167**, 1.
48 T. Nakamura, G. Petzow and L. J. Gauckler, *Mater. Res. Bull.*, 1979, **14**, 649.
49 M. Al Daroukh, V. V. Vashook, H. Ullmann, F. Tietz and I. Arual Raj, *Solid State Ionics*, 2003, **138**, 141–150.
50 M. Crespin, P. Levitz and L. Gatineau, *J. Chem. Soc., Faraday Trans. 2*, 1983, **79**, 1181.
51 M. James and J. P. Attfield, *J. Chem. Soc., Chem. Commun.*, 1994, 1185.
52 F. D. Richardson and J. H. E. Jeffes, *J. Iron Steel Inst.*, 1948, **160**, 261–270.
53 J. C. Burley, P. D. Battle, D. J. Gallon, J. Sloan, C. P. Grey and M. J. Rosseinsky, *J. Am. Chem. Soc.*, 2002, **124**, 620.
54 J. E. Millburn and M. J. Rosseinsky, *J. Mater. Chem.*, 1998, **8**, 1413.
55 M. A. Hayward, *Chem. Mater.*, 2006, **18**, 321.
56 D. Brown, in *Structure and Bonding in Crystals*, ed. M. O'Keefe and A. Navrotsky, Academic Press, New York, 1981, vol. 2, pp. 1–30.
57 N. E. Brese and M. O'Keefe, *Acta Crystallogr., Sect. B: Struct. Sci.*, 1991, **47**, 192.
58 M. Nishijima, Y. Takeda, N. Inanishi, O. Yamamoto and R. Kanno, *J. Jpn. Soc. Powder Metall.*, 1991, **38**, 224–228.
59 S. Tao and J. T. S. Irvine, *Chem. Mater.*, 2006, **18**, 5453.
60 M. Yashima, M. Enoki, T. Wakita, R. Ali, Y. Matsushita, F. Izumi and T. Ishihara, *J. Am. Chem. Soc.*, 2008, **130**, 2762.